

# REPORT DOCUMENTATION PAGE

Form Approved  
OMB No. 0704-0188

Public reporting burden for this collection of information is estimated to average 1 hour per response, including the time for reviewing instructions, searching existing data sources, gathering and maintaining the data needed, and completing and reviewing this collection of information. Send comments regarding this burden estimate or any other aspect of this collection of information, including suggestions for reducing this burden to Department of Defense, Washington Headquarters Services, Directorate for Information Operations and Reports (0704-0188), 1215 Jefferson Davis Highway, Suite 1204, Arlington, VA 22202-4302. Respondents should be aware that notwithstanding any other provision of law, no person shall be subject to any penalty for failing to comply with a collection of information if it does not display a currently valid OMB control number. **PLEASE DO NOT RETURN YOUR FORM TO THE ABOVE ADDRESS.**

**1. REPORT DATE (DD-MM-YYYY)**

30-Sep-2008

**2. REPORT TYPE**

REPRINT

**3. DATES COVERED (From - To)****4. TITLE AND SUBTITLE**

ESTIMATING LOCAL AND NEAR-REGIONAL VELOCITY AND ATTENUATION  
STRUCTURE FROM SEISMIC NOISE

**5a. CONTRACT NUMBER**

FA8718-07-C-0005

**5b. GRANT NUMBER****5c. PROGRAM ELEMENT NUMBER**

62601F

**6. AUTHOR(S)**

Peter Gerstoft<sup>1</sup>, Jian Zhang<sup>1</sup>, William A Kuperman<sup>1</sup>, Nick Harmon<sup>1</sup>, Karim G. Sabra<sup>2</sup>,  
Michael C Fehler<sup>3</sup>, and Steven R Taylor<sup>4</sup>

**5d. PROJECT NUMBER**

1010

**5e. TASK NUMBER**

SM

**5f. WORK UNIT NUMBER**

A1

**7. PERFORMING ORGANIZATION NAME(S) AND ADDRESS(ES)**

University of California at San Diego  
8602 La Jolla Shores Dr.  
La Jolla, CA 92093

**8. PERFORMING ORGANIZATION REPORT  
NUMBER****9. SPONSORING / MONITORING AGENCY NAME(S) AND ADDRESS(ES)**

Air Force Research Laboratory  
29 Randolph Road  
Hanscom AFB, MA 01731-3010

**10. SPONSOR/MONITOR'S ACRONYM(S)**

AFRL/RVBYE

**11. SPONSOR/MONITOR'S REPORT  
NUMBER(S)**

AFRL-RV-HA-TR-2008-1086

**12. DISTRIBUTION / AVAILABILITY STATEMENT**

Approved for Public Release; Distribution Unlimited.

University of California, San Diego<sup>1</sup>, Georgia Institute of Technology<sup>2</sup>, Massachusetts Institute of Technology<sup>3</sup>,  
Rocky Mountain Geophysics, LLC<sup>4</sup>

**13. SUPPLEMENTARY NOTES**

Reprinted from: Proceedings of the 30<sup>th</sup> Monitoring Research Review – Ground-Based Nuclear Explosion Monitoring Technologies, 23 – 25 September 2008, Portsmouth, VA, Volume I pp 57 - 66.

**14. ABSTRACT**

This paper investigates the utility of computing Time-Domain Green's Functions (TDGF) to be used for estimating velocity and attenuation structure for the purposes of nuclear explosion monitoring over local and near-regional distances. Our objective is to extend and apply the methodology of deriving TDGF for propagation between two receivers by cross correlation of seismic noise and/or coda of earthquakes observed at the receivers and concentrates on the following four tasks:

1. The specific noise spectrum of the ocean microseism needs to be accounted for and compensated for in order to be able to measure group velocities across a wider bandwidth. The use of robust time-frequency analysis of the extracted coherent waveforms from seismic noise provides a means to obtain broadband estimates of group velocities up to 0.5 Hz for seismic stations located in coastal regions.

2. We are investigating methods to obtain spatial variations in attenuation using ambient noise. We assume that surface waves generated by atmospheric pressure fluctuations act as a forcing function on a damped harmonic oscillator system. The forcing function is adaptively updated from the network beam as a function of time. The relative attenuation at each site can be estimated from the width of the resonance peak relative to the driving forcing function.

3. Mean-phase velocity-dispersion curves are calculated for the TUCAN seismic array in Costa Rica and Nicaragua from ambient seismic noise using two independent methods, noise cross correlation and beamforming. The noise cross correlation and beamforming methods are compared and contrasted by evaluating results from the TUCAN array. The results of the two methods as applied to the TUCAN array agree within 1%, giving good confidence in the phase velocities extracted from noise.

4. From a data set recorded by a small-scale array (~4 km aperture), unbiased surface-wave Green's functions for short-periods of less than 2 s have been extracted, as evidenced by a good match of noise-based impulse response with the borehole shot records sharing common paths. Beamforming has been used to identify specific directional noise, which may generate fast P-wave arrivals, and thus needs to be analyzed with care. Such noise-based P-wave response and its reflections have turned out to be information-rich as well, revealing the lateral structure anomaly of the studied area.

**15. SUBJECT TERMS**

Seismic noise, Seismic Green's Functions, Cross-correlation

**16. SECURITY CLASSIFICATION OF:**

a. REPORT  
UNCLAS

b. ABSTRACT  
UNCLAS

c. THIS PAGE  
UNCLAS

**17. LIMITATION  
OF ABSTRACT**

SAR

**18. NUMBER  
OF PAGES**

10

**19a. NAME OF RESPONSIBLE PERSON**

Robert J. Raistrick

**19b. TELEPHONE NUMBER (include area  
code)**

781-377-3726

**ESTIMATING LOCAL AND NEAR-REGIONAL VELOCITY AND ATTENUATION  
STRUCTURE FROM SEISMIC NOISE**

Peter Gerstoft<sup>1</sup>, Jian Zhang<sup>1</sup>, William A Kuperman<sup>1</sup>, Nick Harmon<sup>1</sup>, Karim G. Sabra<sup>2</sup>, Michael C Fehler<sup>3</sup>,  
and Steven R Taylor<sup>4</sup>

University of California, San Diego<sup>1</sup>, Georgia Institute of Technology<sup>2</sup>, Massachusetts Institute of  
Technology<sup>3</sup>, Rocky Mountain Geophysics, LLC<sup>4</sup>

Sponsored by Air Force Research Laboratory

Contract No. FA8718-07-C-0005

Proposal No. BAA07-70

**ABSTRACT**

This paper investigates the utility of computing Time-Domain Green's Functions (TDGF) to be used for estimating velocity and attenuation structure for the purposes of nuclear explosion monitoring over local and near-regional distances. Our objective is to extend and apply the methodology of deriving TDGF for propagation between two receivers by cross correlation of seismic noise and/or coda of earthquakes observed at the receivers and concentrates on the following four tasks:

1. The specific noise spectrum of the ocean microseism needs to be accounted for and compensated for in order to be able to measure group velocities across a wider bandwidth. The use of robust time-frequency analysis of the extracted coherent waveforms from seismic noise provides a means to obtain broadband estimates of group velocities up to 0.5 Hz for seismic stations located in coastal regions.
2. We are investigating methods to obtain spatial variations in attenuation using ambient noise. We assume that surface waves generated by atmospheric pressure fluctuations act as a forcing function on a damped harmonic oscillator system. The forcing function is adaptively updated from the network beam as a function of time. The relative attenuation at each site can be estimated from the width of the resonance peak relative to the driving forcing function.
3. Mean-phase velocity-dispersion curves are calculated for the TUCAN seismic array in Costa Rica and Nicaragua from ambient seismic noise using two independent methods, noise cross correlation and beamforming. The noise cross correlation and beamforming methods are compared and contrasted by evaluating results from the TUCAN array. The results of the two methods as applied to the TUCAN array agree within 1%, giving good confidence in the phase velocities extracted from noise.
4. From a data set recorded by a small-scale array (~4 km aperture), unbiased surface-wave Green's functions for short-periods of less than 2 s have been extracted, as evidenced by a good match of noise-based impulse response with the borehole shot records sharing common paths. Beamforming has been used to identify specific directional noise, which may generate fast P-wave arrivals, and thus needs to be analyzed with care. Such noise-based P-wave response and its reflections have turned out to be information-rich as well, revealing the lateral structure anomaly of the studied area.

20081014129



## **OBJECTIVES**

Our objective is to extend and apply the methodology of deriving time-domain Green's functions (TDGF) for propagation between two receivers by cross-correlation of seismic noise and/or coda of earthquakes observed at the receivers. We have previously shown that it is possible to obtain travel-time information for short-period surface waves (around 6 s) by cross-correlating seismic noise at local and regional scales. We propose to add the following improvements to the TDGF method: (1) modifying to better handle cases having nonisotropic noise; (2) implementing a system identification approach for obtaining reliable amplitude information for the TDGF, allowing for the estimation of attenuation along paths between receivers, and (3) extracting TDGF from Lg or Sn coda.

## **RESEARCH ACCOMPLISHED**

### **Improving Surface-Wave Group-Speed Measurements Using Time-Frequency Analysis**

We have previously shown that estimates of the TDGF can be extracted from seismic noise cross-correlation (Sabra et al., 2005a, 2005b). This can be used for measuring local velocity and attenuation structure for the purposes of nuclear explosion monitoring over local and near-regional distances. Using 18 days of seismic noise recording in Southern California, we were able to obtain travel-time information for short-period surface waves (around 7.5 s) by cross-correlating seismic noise at local and regional scales. However, being able to measure broadband estimates of the Rayleigh wave group velocity can potentially provide a means to better constrain the inversion procedure about crustal velocity structure.

We have investigated signal-processing tools to improve the measurements of group-speed estimates from the cross-correlation waveforms. Surface waves are dispersive, and their associated dispersion curves can be used to invert for shear velocity profiles with depth. The main challenge with using surface waves is the complexity of the required data processing and interpretation of the results. Our goal is to show how robust time-frequency analysis of the extracted coherent waveforms from seismic noise improves the precision of group velocity measurements of surface waves. In particular, it is important to reduce the uncertainty of the dispersion-curve measurements in order to minimize the number of acceptable earth models.

Group velocities are typically measured by computing spectrograms or the moving-window method. In seismology they are often estimated using multiple filter banks. All these techniques result from Fourier transforms and thus create a large smearing in the time–frequency domain as a result of the Gabor-Heisenberg inequality (Gabor, 1946). An additional issue is the biases caused by the seismic signals' being nonstationary and strongly varied in spectral amplitude. To mitigate those limitations, various time–frequency methods have been developed (Cohent, 1989). The Wigner-Ville transform  $WV_{lm}(t,f)$  yields a time-frequency energy distribution of the cross-correlation  $C_{lm}(t)$  (with analytic representation noted  $\tilde{C}_{lm}$  [Auger and Flandrin, 1995]) computed between two seismic noises recorded at sensors #l and #m:

$$WV_{lm}(t, f) = \int_0^T \tilde{C}_{lm}(t + \tau/2) \tilde{C}_{lm}^*(t - \tau/2) \exp(-i2\pi f\tau) d\tau . \quad (1)$$

We tested his approach on the cross-correlation waveform obtained from seismic noise recorded southwest of the Hawaiian Islands (Laske, 1999). Seismic months of seismic noise (June 1997 to December 1997) were recorded on a pair of OBS sensors, 342 km apart, and sampled at 25 Hz. The seismic cross-correlation was computed following the methodology described in (Sabra et al. 2005a). We computed the Wigner Ville transform using the algorithm described in (Auger and Flandrin, 1995). In order to ease the visual interpretation of the signal's time-frequency structure, a smoothed version can be computed by a two-dimensional (2D) low-pass filtering of the Wigner-Ville transform in order to reduce the interference of cross terms and noise artifacts (Figure 1.a). Selecting the arrival times along the maxima contours of the  $WV_{lm}(t,f)$  yields an estimate of the change of the group velocity  $V_g$  vs. frequency  $f$ , of these coherent seismic waves between sensor pairs. As a complement to this smoothing, a reassigned representation of  $WV_{lm}(t,f)$  is performed that essentially increases the concentration of the signal components (Figure 1.b) (Auger and Flandrin, 1995), thus improving estimates of  $V_g$ . Extracting reliable and high-resolution measurements of

$V_g$  are essential for the estimation of the earth velocity structure. Robust time-frequency analysis of the extracted coherent waveforms from seismic noise, appear to provide broadband estimates of group velocities up to at least 0.25 Hz for seismic stations located in coastal regions.

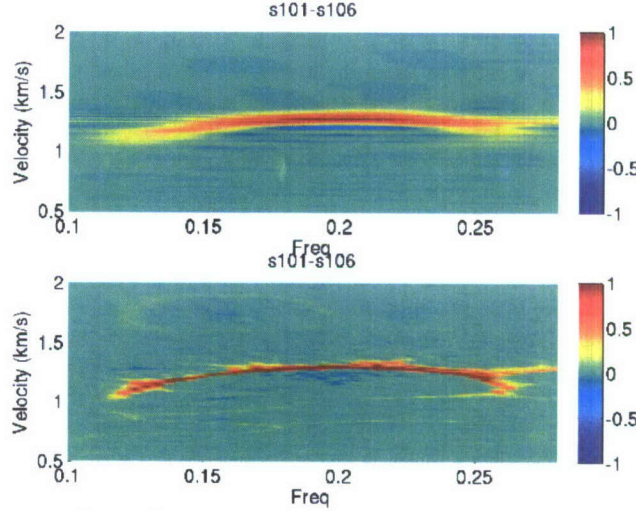


**Figure 1. Time-frequency analysis of the extracted coherent between a pair of OBS sensors located 343 km apart southwest of the Hawaiian Islands: (a) smoothed Wigner-Ville transform and (b) Wigner-Ville transform after energy reassignment processing.**

#### Extracting Attenuation from Noise

We have been using ambient seismic noise to construct attenuation maps beneath a network of stations. The approach we are looking at is to estimate the  $Q$  on a site-by-site basis as opposed to taking a tomographic approach (e.g., Matzel, 2008). The idea is to treat time-varying frequency-wavenumber (F-K) beams of the ambient noise field as a forcing function beneath a network of stations. Each station responds differently to the forcing function, depending on the site structure and attenuation. We use the differential equation for a forced, damped, harmonic oscillator to simulate the response of each station to the forcing function given by

$$\ddot{x} + \gamma \dot{x} + \omega_0^2 x = \frac{1}{m} F(t), \quad (1)$$

where  $F(t)$  is the forcing function,  $m$  is the mass,  $x$  is the sensor displacement response to the forcing function,  $\gamma$  is the viscous damping term, and  $\omega_0$  is the natural frequency of the oscillator. The power spectrum of the sensor response (where  $m = 1$ ) is given by

$$P_x(\omega) = \frac{P_F(\omega)}{\left[ (\omega_0^2 - \omega^2)^2 + (\gamma\omega)^2 \right]}. \quad (2)$$

As will be further described below, we estimate the power spectrum of the forcing function from the array beam on the maximum power of the ambient noise field. For light damping,  $\gamma \ll \omega_0$ , the power spectrum for a particular site relative to that of the forcing function is given by

$$P_{xF}(\omega) = \frac{P_x(\omega)}{P_F(\omega)} = \frac{1}{\omega_0^2 \left[ 4(\omega_0^2 - \omega^2)^2 + \left( \frac{\omega}{Q} \right)^2 \right]}, \quad (3)$$

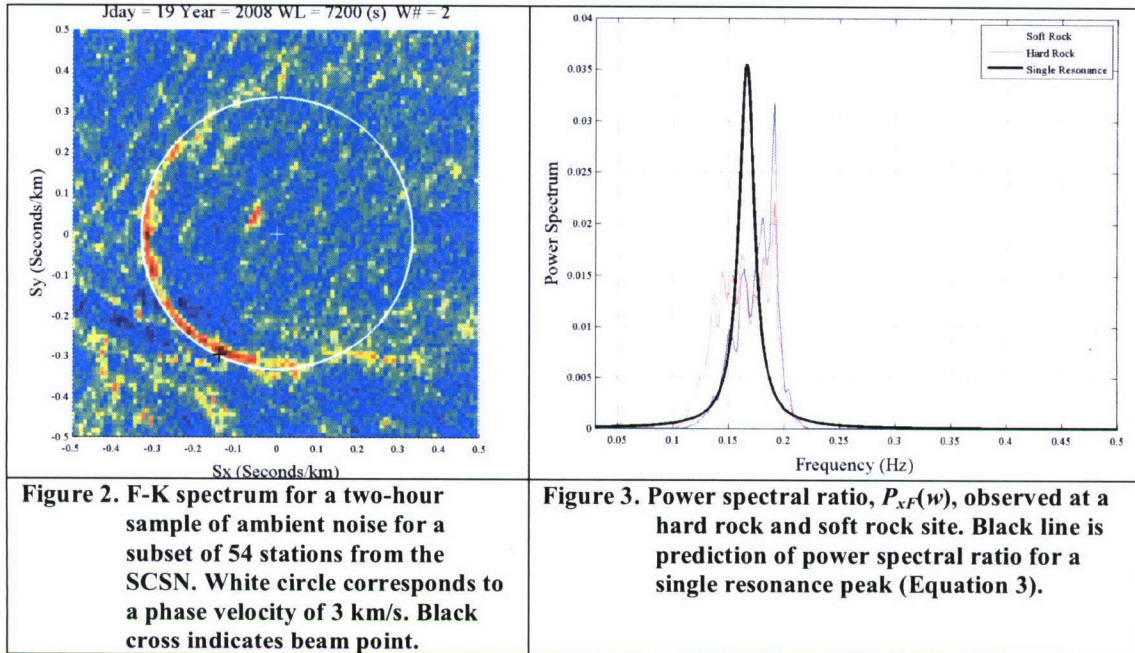
where  $\gamma = \omega_0/Q$ . For each station, it is then possible to do a grid search over a range of  $\omega_0$  and  $Q$  values to match the observed resonance peaks.



To find the power spectrum of the forcing function,  $P_F(\omega)$ , we first compute the time varying F-K spectrum of the ambient noise impinging upon a network of stations. To test the methodology, we examined one day's worth of noise for a subset of 54 stations from the Southern California Seismic Network (SCSN). We computed the F-K spectrum for two-hour window lengths, an example of which is shown in Figure 2.

The noise predominantly arrives from the west and southwest for this particular time block. The black cross in Figure 2 shows the point having the maximum energy for the F-K spectrum, and we computed a beam from this point. In future work, we will examine the possibility of integrating a semicircle of beams from the F-K spectrum spanning a wider range of azimuths. In our preliminary study, we have computed the beams from the maximum F-K point for each of the two-hour time windows and computed the median power for the day as a power spectral estimate of the forcing function. Using the F-K beam and the median power appears to eliminate the necessity of one-bit normalization commonly used to remove earthquakes from ambient noise-time series.

Figure 3 shows the observed power spectral ratio,  $P_{xF}(\omega)$ , at a hard-rock (CHF) and soft-rock (BRE) site. Note that the resonance curve for the soft-rock site is broader than that from the hard-rock site indicating higher attenuation at the soft-rock site. The solid line in Figure 3 shows the predicted resonance peak for a single oscillator frequency (Equation 4). The prediction appears to be too peaked, suggesting that a more general absorption band model (e.g., Liu, 1976) may be necessary to fit the observed resonance peaks.



#### Midscale Seismic Beamforming and Noise Cross-Correlation

We determined phase velocities using 593 days (July 2004 to March 2006) of station-to-station noise cross-correlation function (NCF) for the vertical components of the 49 stations of the TUCAN seismic array (Figure 4c) using a method similar to Harmon et al. (2007). Variations from Harmon et al. (2007) include removing the instrument responses from the signals (the TUCAN contains different sensor types), decimation to 1-s sampling, a root mean square (RMS) clipping scheme for the daily time series (Sabra et al., 2005) and signal whitening by normalizing the Fourier coefficients by their respective magnitude, both to create a single broadband NCF. Then we cross-correlated hourly time series segments for all station pairs and stacked the resulting correlograms. The NCF phase dispersion was determined by unwrapping the phase of the stacked NCF and applying a  $\pi/4$  correction. We determined the cycle ambiguity by matching the average phase velocity determined from teleseismic events at 20-s periods (Abers et al., 2007). The mean teleseismic phase velocity estimates were determined using the method of Yang and Forsyth (2006),



with 95 events with good azimuthal coverage. We calculate the mean phase dispersion curve and its standard error of the mean by station-to-station distance-weighted averaging. A station-to-station NCF phase velocity estimate was used to calculate the mean phase dispersion curve if (1) the NCF had signal-to-noise ratio  $>10$ , (2) the temporal average of  $\sim 4$ -month NCF stacks had a standard deviation of  $<1$  km/s, and (3) the station-to-station path was greater than  $3\lambda$  after Lin et al. (2008). Distance weighting was chosen since longer paths should be more representative of average structure. For 15–29-s periods, the teleseismic and NCF mean phase velocity estimates were within 1%, except at 18 s, where they were within 2%.

For station-to-station paths perpendicular to the Pacific coast, the NCFs are dominated by 6–10-s microseisms coming from the coast. This can be seen by comparing NCFs with comparable path lengths and different orientations such as N1–N13 and B4–N11 (Figure 4f, e). A high-frequency signal owing to the Pacific microseisms is seen at negative lag (from southwest) for the path perpendicular to the Pacific coast whereas no high-frequency signal is seen at positive lag for this path (Figure 4f) or for positive and negative lags of the coast parallel paths (Figure 4d, e). The amplitudes and frequency contents of the NCFs suggest that the noise distribution changes with period.

For periods between 10 and 22 s, the Beamformer output in Figure 5, there is a nearly continuous ring maximum with surface wave slownesses, suggesting that surface waves dominate the signal in this period range, which is consistent with the 2D model of noise distribution. Above a 18-s period, there is little signal from the Pacific ( $180^\circ$ – $240^\circ$ ), while in the secondary microseism band (6–10-s period) the dominant source direction is  $180^\circ$ – $240^\circ$  azimuth with little energy coming from other directions, which is consistent with what was observed in the NCF.

For periods greater than 6 s, both NCF and beamformer average phase-velocity estimates are within an error of each other (Figure 6). For the best-resolved periods (7–20 s), the phase velocity from beamforming agrees within 1% with the NCF estimates. The agreement is best in this band because this is where the microseisms are strongest (see Figure 5). Below a 6-s period, the agreement between the two estimates begins to erode due to aliasing, as the beamformer output no longer resolves any coherent surface waves, and the errors in the NCF estimates increase. The NCF estimate is more stable due to the inherent averaging in the frequency domain caused by windowing in the time domain. The station geometry requirements for the two methods are different. The NCF method requires only two stations. Beamforming, on the other hand, requires an array of stations. We choose the NCF station spacing to be at least  $3\lambda$  at a 20-s period to avoid near-field effects and to allow distinct phases to emerge (Bensen et al., 2007). Data selection requirements of the NCF limit the number of station pairs to 270 out of 1149 at 20 s. For beamforming array aperture larger than  $1\lambda$  is required to resolve the longest periods of interest and station spacing  $< \lambda/2$  to prevent spatial aliasing at shortest periods for a regularly spaced array, but for irregular arrays it can be relaxed somewhat. For the TUCAN array, which consists mainly of two regularly-spaced line arrays pointing southwest, beamforming aliasing manifests itself as a straight-line beamformer output (perpendicular to the line-array directions) rather than a point for sources coming from the southwest, as shown in the 7-s band in Figure 5. For shorter periods, the beamformer aliasing becomes more severe, making it difficult to extract phase velocities. In the 7–20-s bands, the phase slowness can be resolved, but aliasing does contribute to the errors in the phase-slowness estimates. Overall, the aliasing at the periods of interest, 7–20 s, is minor, while it dominates at periods of less than 7 s.

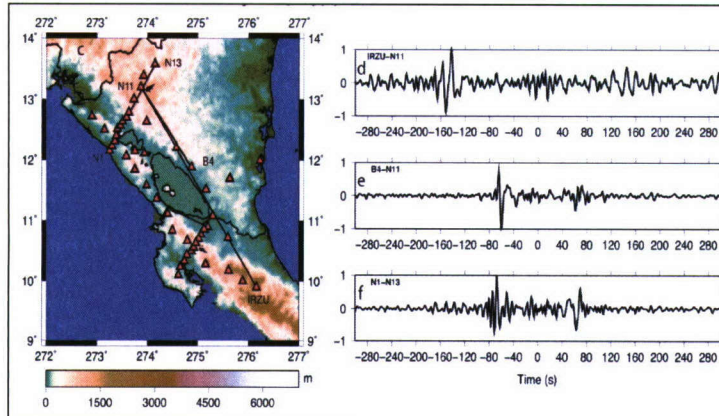


**Figure 4.** Station locations (red triangles) and topography (from ETOPO2) of the TUCAN array. The time series show the normalized bandpass filtered (5–33 s) NCF between stations (d) IRZU-N11, (e) B4-N11, and (f) N1-N13. Positive lags correspond to waves traveling from N11 and N13.

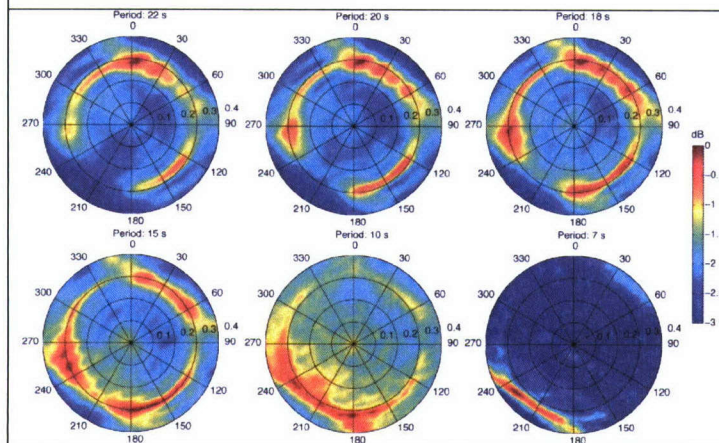


**Figure 5.** Azimuth vs. phase slowness plots of 593-day stack of beamformer output (dB) of the TUCAN array for 7-, 10-, 15-, 18-, 20-, and 22-s periods. Slowness is the radial distance on the polar plots from 0.00–0.4 s/km.

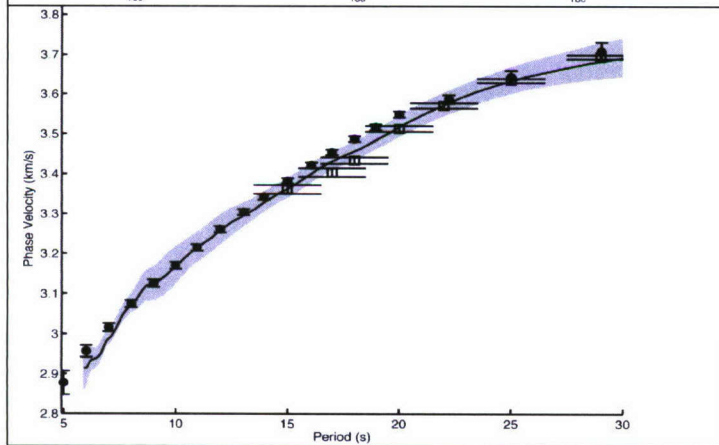


**Figure 6.** Phase-velocity estimates from beamforming (solid black line), with 3 $\times$  standard error of the mean (grey region), noise correlation methods (circles), with 3 $\times$  standard error of the mean bars and teleseismic phase-velocity estimates (open squares), with 3 $\times$  standard error of the mean.

### Local-Scale Seismic Noise Cross-Correlation from the Calico Fault Experiment

In this work we present the seismic noise cross-correlation (NCC) results from a dataset recorded by a dense array (~5-km aperture, see Figure 7a) along the Calico fault in California's Mojave desert. The dataset is unique for NCC study in terms of (1) local scale (a few km), (2) long recordings (~6 months), and (3) the common site of a sensor and a borehole shot, allowing direct comparison of the noise-based Green's functions with the shot records. Our goal is to demonstrate the successful retrieval of reliable Green's functions from a noise field with a strong P-wave component and the application of seismic NCC for revealing fault zone structures.



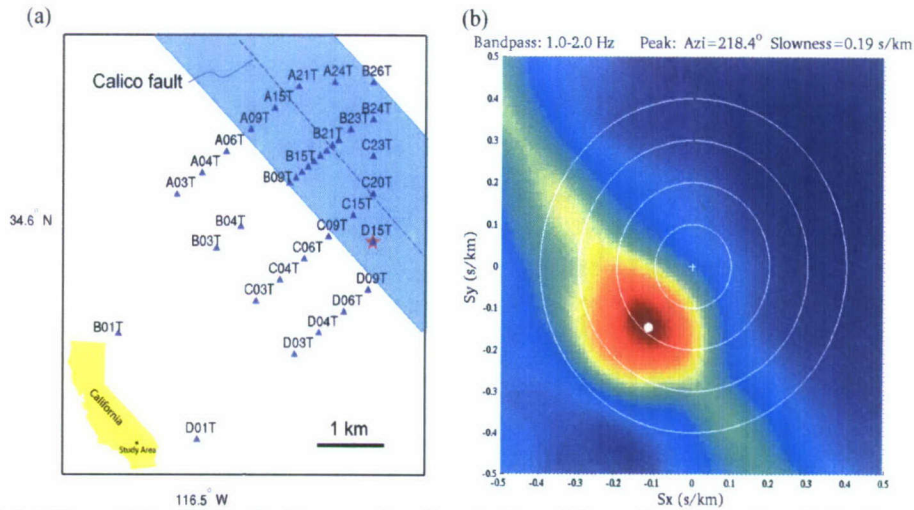


**Figure 7. (a) Map of the Calico fault area, showing stations (blue triangles), a borehole shot (red star), the Calico fault trace (dashed), and the fault zone (light blue); (b) Slowness-azimuth distribution of the noise field from beamforming, stacked over a frequency band of 1–2 Hz.**

Over broadband, the major part of the noise in southern California are microseisms mainly coming from the Pacific ocean (e.g., Gerstoft and Tanimoto, 2007). Here we focus on the frequency band of 0.5–3.0 Hz, in which microseisms may not be predominant. Using vertical-component noise records, we show in Figure 7b a 1-day beamforming output stacked over 1.0–2.0 Hz. Clearly the noise field is dominated by a coherent energy coming from the SW, at an apparent speed of  $\sim 5$  km/s. Such slowness-azimuth pattern holds for all the other days within the 6-month period, indicating that this incident energy is temporally and spatially stable. Given the apparent speed of  $\sim 5$  km, it is too fast to be a surface wave. We further suggest that it is a P wave as it is strongest on the vertical component.

From beamforming results, apparently a plane wave arrives at the array from the lower crust or upper mantle. We then expect to see a peak in the NCC output of a pair of sensors, of which the time lag from zero corresponds to the effective interreceiver distance along the direction of the incident wave, rather than the one along the surface. The time when the peak emerges would be a cosine function of the difference between the azimuths of the station-pair axis and the incident wave. Note, that for the case of a body wave, such a peak is no longer related to neither surface-wave nor body-wave Green's function. However, we still expect to see surface-wave Green's functions in the NCC outputs, as long as a diffusive wavefield (at least partially) coexists.

Indeed, we observe both a fast- and a slow-wave packet in the NCC output of each pair. Both appear propagating from the record section (not shown) of the NCC traces having directions roughly along NE–SW. The fast wave packet has a speed of about 5 km/s (getting faster for station pairs with azimuths away from NE–SW, e.g., arriving at zero along NW–SE), confirming that it is originated from the ballistic body wave observed from beamforming. The slow one turns out to be a packet of surface-wave Green's functions, as verified by a good match, for a range of distance and azimuth, respectively, of the noise-based impulse responses (the derivative of NCC outputs) with the records of a borehole shot sharing common paths (Figure 8). This comparison is a particular advantage of our experiment as we deployed a sensor (D15T in Figure 7a) at essentially the same site as the shot (red star in Figure 7a).



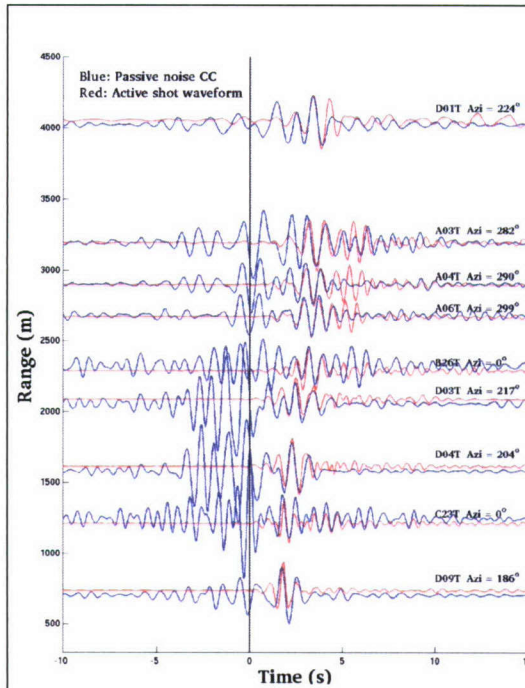


**Figure 8.** A good match of noise-based surface-wave Green's functions (blue) with the borehole shot records sharing common paths.

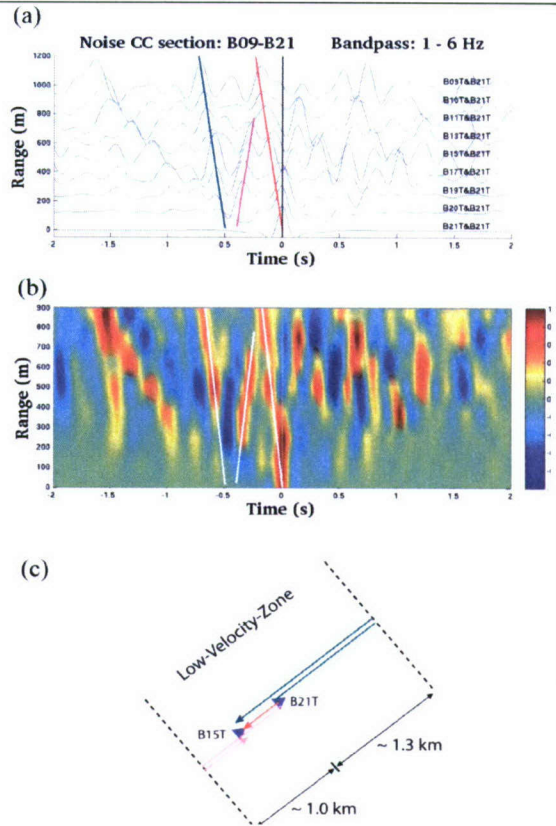


**Figure 9.** (a) Record section of the NCC, for the profile B09T-B21T. Lines of red, purple, and green mark the direct arrival and its reflections from the side walls of LVZ, respectively. (b) Same as in (a), except the amplitude of the signals shown in color scale. (c) An LVZ model showing an example of the corresponding virtual arrivals from B21T to B15T.

Our results indicate that the NCC technique is feasible and robust in converging Green's functions even for the noise field dominated by strong ballistic waves. However, caution is needed to distinguish body-wave Green's functions from plane-wave generated impulse responses. Although the case we provided is for near-field, i.e., scales less than a few wavelengths, which means that specific modes of surface waves are not well developed yet, Green's functions emerged from noise may still find their applications in exploration, engineering, and explosion monitoring fields, e.g., surface-wave isolation/removal.

The P-wave noise identified in our experiment provides a stable natural source for studying the structures along the Calico fault. By performing NCC for pairs of sensors along a profile (B09T-B21T, see Figure 7a), we construct a virtual record-section (Figure 9a) as if a plane-wave source with an apparent speed of 5 km/s were placed at the site of B21T. Interestingly, as seen in Figure 9a and 9b, besides the direct arrival of the virtual event (marked by a red line), another two arrivals with the same absolute speed show up (marked by a purple line and a green line, respectively). Indeed, these three arrivals can be interpreted by a low-velocity-zone (LVZ) model shown in Figure 9c. Thus, the wave from a virtual source at B21T will be reflected back from both sides of the boundaries of LVZ. From the direct arrival and its reflections in the record-section, our inversion of the distance from B21T to the reflectors (i.e., side walls of LVZ) amounts

to 1.0 km and 1.3 km, respectively. Thus, we estimate that the width of the Calico fault LVZ to be about 2.3 km, which agrees favorably with other evidences (Radiguet, unpublished material).

### **CONCLUSIONS AND RECOMMENDATIONS**

- (1) Using time-frequency analysis methods, more-robust estimates of the surface-wave group velocity can be obtained.
- (2) Seismic attenuation near a station can be extracted from noise by assuming that the ambient noise obtained from a time-variable F-K beam acts as a forcing function on a damped harmonic oscillator system.
- (3) Beamformer output provides valuable information about noise distribution through time. We show that from 7–20-s period seismic noise in clipped seismograms for 18 months of data is dominated by surface waves and is consistent with a 2D model of noise distribution, having good azimuthal coverage from 10–22-s period. Beamforming provides an accurate, independent estimate of the mean phase-velocity dispersion across a seismic array that is within 1% of NCF and teleseismic estimates. Thus, beamforming can potentially resolve the cycle ambiguity in NCF phase-velocity estimates without a complementary teleseismic study.
- (4) We provide results of a local-scale ( $\sim 5 \text{ km} \times 5 \text{ km}$ ) seismic NCC experiment at a frequency band of 0.5 Hz and above. By applying beamforming, we identify a strong P wave in the noise field, suggesting that a careful analysis of the noise distribution and wave type is needed in the efforts of extracting P-wave Green's functions. By comparing the noise-based surface-wave Green's functions with the borehole shot records sharing common paths, we obtain a good match and thus verify the robustness of the NCC technique for a noise field dominated by a body wave. We then find that the NCC can turn the ballistic P-wave noise into a virtual record-section of a profile of sensors. From the direct arrival and its reflections shown in the record section, we invert the width of the Calico fault LVZ to be  $\sim 2.3 \text{ km}$ .

### **REFERENCES**

- Abers, G. A., K. M. Fischer, M. Protti, and W. Strauch (2007). The TUCAN broadband seismometer experiment: Probing mantle melting in the Nicaragua-Costa Rica subduction zone, *IRIS Newsletter* 1: 10–12.
- Auger, A. and P. Flandrin (1995). Improving the readability of time-frequency and time-scale representations by the reassignment method, *IEEE Trans. Sig. Process.* 43: 1068–1089.
- Bensen, G. D., M. H. Ritzwoller, M. P. Barmin, A. L. Levshin, F. Lin, M. P. Moschetti, N. M. Shapiro, and Y. Yang (2007). Processing seismic ambient noise data to obtain reliable broadband surface wave dispersion measurements, *Geophys. J. Int.* 169: doi: 10.1111/j.1365-1246X.2007.03374.x.
- Cohen, L. (1989). Time-frequency distribution—A review, *Proc. IEEE* 77: 941–981.
- Gabor, D. (1946). Theory of communication, *J. Inst. Electron. Eng.* 93: 429–457.
- Gerstoft, P. and T. Tanimoto (2007). A year of microseisms in southern California, *Geophys. Res. Lett.* 34: L20304, doi:20310.21029/22007GL031091.
- Harmon, N., D. Forsyth, and S. Webb (2007). Using ambient seismic noise to determine short-period phase velocities and shallow shear velocities in young oceanic lithosphere, *Bull. Seis. Soc. Am.* 97: 2024–2039.
- Laske, G., J. Phipps Morgan, and J. A. Orcutt, (1999). First results from the Hawaiian SWELL pilot experiment: *Geophys. Res. Lett.* 26: 3397–3400, doi: 10.1029/1999GL005401.
- Lin, F., M. P. Moschetti, and M. H. Ritzwoller (2008). Surface wave tomography of the western United States from ambient seismic noise: Rayleigh and Love wave phase velocity maps, *Geophys. J. Int.*, doi:10.1111/j.1365-1246X.2008.03720.x.



- Liu, H. P., D. L. Anderson, and H. Kanamori (1976). Velocity dispersion due to anelasticity: Implications for seismology and mantle composition, *Geophys. J. R. Astron. Soc.* 47: 41–58.
- Matzel, E. M. (2008). Attenuation tomography using ambient noise correlation, *Seism. Res. Lett.* 79: 358.
- Sabra, K., P. Gerstoft, P. Roux, W. A. Kuperman, and M. Fehler (2005a). Extracting time-domain Green's function estimates from ambient seismic noise, *Geophys. Res. Lett.* 32.
- Sabra, K., P. Gerstoft, P. Roux, W. A. Kuperman, and M. Fehler (2005b). Surface wave tomography from microseisms in Southern California, AGU *Geophys. Res. Lett.* 32: L14311, doi:10.1029/2005GL023155.
- Yang, Y. and D. W. Forsyth (2006). Regional tomographic inversion of amplitude and phase of Rayleigh waves with 2-D sensitivity kernels, *Geophys. J. Int.* 166: 1148–1160.